Available online at www.sciencedirect.com
SCIENCE DIRECT®
Journal of Hydrology 275 (2003) 208–228
Journal of Hydrology
www.elsevier.com/locate/jhydrol

Applications of nonstationary stochastic theory to solute transport in multi-scale geological media

Jichun Wu[a,b], Bill X. Hu[a,*], Dongxiao Zhang[c]

[a]*Desert Research Institute, Division of Hydrologic Sciences, University and Community System of Nevada, 755 E. Flamingo Road, Las Vegas, NV 89119, USA*
[b]*Nanjing University, Department of Earth Sciences, Nanjing, People's Republic of China*
[c]*Hydrology, Geochemistry, and Geology Group, Earth and Environmental Sciences, Los Alamos National Laboratory, Los Alamos, NM, USA*

Received 17 March 2001; accepted 17 January 2002

Abstract

In this study, we make use of a nonstationary stochastic theory in studying solute flux through spatially nonstationary flows in porous media. The nonstationarity of flow stems from various sources, such as multi-scale, nonstationary medium features and complex hydraulic boundary conditions. These flow nonstationarities are beyond the applicable range of the 'classical' stochastic theory for stationary flow fields, but widely exist in natural media. In this study, the stochastic frames for flow and transport are developed through an analytical analysis while the solutions are obtained with a numerical method. This approach combines the stochastic concept with the flexibility of the numerical method in handling medium nonstationarity and boundary/initial conditions. It provides a practical way for applying stochastic theory to solute transport in complex groundwater environments. This approach is demonstrated through some synthetic cases of solute transport in multi-scale media as well as some hypothetical scenarios of solute transport in the groundwater below the Yucca Mountain project area. It is shown that the spatial variations of mean log-conductivity and correlation function significantly affect the mean and variance of solute flux. Even for a stationary medium, complex hydraulic boundary conditions may result in a nonstationary flow field. Flow nonstationarity and/or nonuniform distribution of initial plume (geometry and/or density) may lead to nonGaussian behaviors (with multiple peaks) for mean and variance of the solute flux. The calculated standard deviation of solute flux is generally larger than its mean value, which implies that real solute fluxes may significantly deviate from the mean predictions.

1. Introduction

Most stochastic theories (e.g. Dagan, 1989; Gelhar, 1993; Cushman, 1997) for groundwater flow and solute transport in porous formations are developed under the following assumptions: (1) a steady-state flow with no boundaries (or infinite boundaries), (2) a stationary hydraulic conductivity field, (3) a uniform mean velocity in space; and (4) simple initial conditions for solute plume, such as a point source or rectangular box with instant or step release. Violation of any of the first three assumptions will render the groundwater flow field nonstationary in space. Some cases of regional groundwater flows under natural conditions may be treated as steady-state flows with infinite boundaries. However,

* Corresponding author. Tel.: +1-702-895-0438; fax: +1-702-895-0427.
E-mail address: hu@dri.edu (B.X. Hu).

0022-1694/03/$ - see front matter © 2003 Elsevier Science B.V. All rights reserved.
doi:10.1016/S0022-1694(03)00044-1

the assumption of constant mean velocity is generally not valid, and is only suitable at some specific regions (or zones). The assumption of conductivity stationarity may be appropriate within a single geologic formation. Simple plume initial condition may be representative for some special cases, such as the controlled field experiments at Borden, Canada and Cape Cod, Massachusetts (Sudicky, 1986; Hess, 1989; Graham and McLaughlin, 1989a,b]. Adoption of these assumptions can significantly simplify mathematics for flow and transport calculations. We call the theories based on these assumptions, the classical stochastic theories. However, many flow fields and chemical transports do not satisfy the assumptions listed above. The prediction by the classical theories may significantly deviate from actual field findings. Recently, some of these assumptions have been relaxed and stochastic models are gradually extended to more complicated cases.

Indelman and Yubin (1996) developed a Lagrangian resident concentration theory for solute transport in nonstationary flow fields and applied it to the case of transport in media displaying a linear trend in the mean log hydraulic conductivity field. Flow nonstationarity caused by this special case of medium nonstationarity has been extensively studied in the literature (e.g. Rubin and Seong, 1994; Indelman and Rubin, 1995; Li and McLaughlin, 1995; Zhang, 1998). Recently, Zhang et al. (2000) developed a general theoretical framework for solute flux through spatially nonstationary flows in porous media. The solute flux method is used to evaluate the solute travel time and transverse displacement through a fixed control plane downstream of the solute source. The solute flux statistics (mean and variance) are derived through a Lagrangian perturbation method and are expressed in terms of the probability density functions (PDFs) of particle travel time and transverse displacement. These PDFs are evaluated with the first two moments of travel time and transverse displacement under the assumed solute distribution form.

In this study, Zhang et al.'s (2000) theory is applied to groundwater flow and solute transport under complex hydrogelogical conditions. We will first use hypothetical cases to study the influences of flow nonstationarity and initial plume distribution on solute transport. The flow nonstationarity stems from the existence of zones in the medium and/or nonuniform mean flow caused by the limited boundaries. Owing to the complex flow, and initial and boundary conditions, a numerical method is used to solve the governing equations derived from the analytical analysis. This approach combines the stochastic concept with the flexibility of numerical methods, so that it can deal with much more complex flow and transport problems than the classical theories, and at the same time, it greatly decreases the computational time in comparison with Monte Carlo numerical simulation. The developed method is later applied to solute transport in the groundwater below the Yucca Mountain project area in Nevada. The study results exhibit the significant influence of the flow nonstationarity on solute transport, and show the importance of the nonstationary transport theory to real environmental projects.

2. Stochastic formulation of solute mass flux

We consider incompressible groundwater flow in a heterogeneous aquifer with spatially variable hydraulic conductivity $K(\mathbf{x})$, where $\mathbf{x}(x, y, z)$ is a Cartesian coordinate vector. Groundwater seepage velocity, $\mathbf{V}(\mathbf{x})$, satisfies the continuity equation, $\nabla\cdot(n\mathbf{V}) = 0$, and Darcy's law, $\mathbf{V} = -(K/n)\nabla h$, where n is the effective porosity, and h is the hydraulic head. The $\mathbf{V}(\mathbf{x})$ is considered to be nonstationary caused by the medium nonstationarity and/or bounded domain. A solute of total mass M is released into the flow field at time $t = 0$, over the injection area A_0 located at $x = 0$, either instantaneously or with a known release rate quantified by a rate function, $\phi(t)[T^{-1}]$. We denote with $\rho_0(\mathbf{a})[M/L^2]$ an areal density of injected solute mass at the location $\mathbf{a} \in A_0$. With $\Delta\mathbf{a}$ denoting an elementary area at $\mathbf{a}$, the particle of mass $\rho_0\Delta\mathbf{a}$ is advected by the random spatially nonstationary groundwater velocity field $\mathbf{V}$. The total advected solute mass is $M = \int_{A_0} \rho_0 d\mathbf{a}$. If the solute mass is uniformly distributed over A_0, then $\rho_0 = M/A_0$. For $t > 0$, a solute plume is formed and advected downstream by the flow field toward a (y, z)-plane, located at some distance from the source, through which the solute mass flux is to be predicted or measured. The plane is referred to as the control plane (CP). For nonreactive solute, integrating the solute flux for a single particle, $\Delta q \equiv \rho_0(\mathbf{a})d\mathbf{a}\phi(t-\tau)\delta(\mathbf{y}-\boldsymbol{\eta})$,

over the injection area A_0, averaging over the sampling area $A(\mathbf{y})$ centered at $\mathbf{y}(y,z)$, yields the solute mass flux component orthogonal to the CP at x as

$$q(t,\mathbf{y};x,A)=\frac{1}{A}\int_{A_0}\int_{A}\rho_0(\mathbf{a})\phi(t-\tau)\delta(\mathbf{y}'-\boldsymbol{\eta})\mathrm{d}\mathbf{y}'\mathrm{d}\mathbf{a} \quad (1)$$

where $\tau\equiv\tau(x;\mathbf{a})$ is the travel time of the advective particle from $\mathbf{a}$ to the control plane at x, and $\boldsymbol{\eta}\equiv(\eta,\xi)$, ($\eta\equiv\eta(x;\mathbf{a})$ and $\xi\equiv\xi(x;\mathbf{a})$) are the transverse locations of a particle passing through the CP.

The quantities τ and η in Eq. (1) are random variables and are functions of the underlying random velocity field. The expected value of q in Eq. (1) in the case of point sampling (i.e. $A\rightarrow 0$) can be expressed as (Zhang et al., 2000),

$$\langle q(t,x)\rangle=\int_{A_0}\int_0^\infty\rho_0(\mathbf{a})\phi(t-\tau)f_1[\tau(x,\mathbf{a})=t\boldsymbol{\eta}(x,\mathbf{a})=\mathbf{y}]\mathrm{d}\tau\mathrm{d}\mathbf{a} \quad (2)$$

where $\mathbf{x}=(x,\mathbf{y})$ and $f_1[\tau(x,\mathbf{a}),\eta(x,\mathrm{a})]$ denotes the joint probability density function (PDF) of travel time τ for a particle from $\mathbf{a}$ to reach x and the corresponding transverse displacement η. The variance of the solute flux for the point sampling is evaluated as

$$\sigma_q^2(t,x)=\langle q^2(t,x)\rangle-\langle q(t,x)\rangle^2 \quad (3)$$

with

$$\langle q^2(t,x)\rangle=\int_{A_0}\int_{A_0}\int_0^\infty\int_0^\infty\rho_0(\mathbf{a})\rho_0(\mathbf{b})\times\phi(t-\tau_1)\phi(t-\tau_2)f_2[\tau_1(x,\mathbf{a})=t,\boldsymbol{\eta}_1(x,\mathbf{a})=\mathbf{y};\tau_2(x,\mathbf{b})=t,\boldsymbol{\eta}_2(x,\mathbf{b})=\mathbf{y}]\mathrm{d}\tau_1\mathrm{d}\tau_2\mathrm{d}\mathbf{a}\mathrm{d}\mathbf{b} \quad (4)$$

where $f_2[\tau_1(x,\mathbf{a}),\eta_1(x,\mathbf{a});\tau_2(x,\mathbf{b}),\eta_2(x,\mathbf{b})]$ is the two-particle joint PDF of travel time and transverse displacement. For the special case of stationary flow the PDFs do not depend on the absolute locations of the starting point $\mathbf{a}(a_x,a_y,a_z)$ and CP location, but depend on their relative distance. In stationary flows, $\tau(x;\mathbf{a})$ and $\boldsymbol{\eta}(x;\mathbf{a})$ are uncorrelated, at least up to the first-order in the variance of log-conductivity (Dagan et al., 1992), and thus $f_1[\tau,\boldsymbol{\eta}]=f_1[\tau]f_1[\boldsymbol{\eta}]$. This assumption was later extended to the two-particle joint PDF (Andricevic and Cvetkovic, 1998), that is, $f_2[\tau_1,\eta_1;\tau_2,\eta_2]=f_2[\tau_1,\eta_1]f_2[\tau_2,\eta_2]$. However, this assumption is not suitable to solute transport in a nonstationary flow (Zhang et al., 2000).

The solute discharge is another quantity of interest defined as the total solute mass flux over the entire CP at x,

$$Q(t,x)=\int_{A_0}\int_{\mathrm{CP}}\rho_0(\mathbf{a})\phi(t-\tau)\delta(y-\eta)\mathrm{d}\mathbf{a}\mathrm{d}y \quad (5)$$

where $\mathbf{y}$ is a point in the CP. Its mean and variance are given as

$$\langle Q(t,x)\rangle=\int_{A_0}\int_0^\infty\rho_0(\mathbf{a})\phi(t-\tau)f_1[\tau(x,\mathbf{a})]d\tau d\mathbf{a} \quad (6)$$

$$\sigma_Q^2(t,x)=\langle Q^2(t,x)\rangle-\langle Q(t,x)\rangle^2 \quad (7)$$

$$\langle Q^2(t,x)\rangle=\int_{A_0}\int_{A_0}\int_0^\infty\int_0^\infty\rho_0(\mathbf{a})\rho_0(\mathbf{b})\times\phi(t-\tau_1)\phi(t-\tau_2)f_2[\tau_1(x,\mathbf{a});\tau_2(x,\mathbf{b})]d\tau_1 d\tau_2 d\mathbf{a}d\mathbf{b} \quad (8)$$

where $f_1[\tau(x,\mathbf{a})]$ is the marginal PDF of $f_1[\tau(x,\mathbf{a}),\eta(x,\mathbf{a})]$, and $f_2[\tau_1(x,\mathbf{a});\tau_2(x,\mathbf{b})]$ is the marginal PDF of $f_2[\tau_1(x,\mathbf{a}),\boldsymbol{\eta}_1(x,\mathbf{a});\tau_2(x,\mathbf{b}),\boldsymbol{\eta}_2(x,\mathbf{b})]$.

3. Joint probability density functions

To evaluate the statistical moments of solute flux, one needs to know the one- and two-particle PDFs f_1 and f_2, or an infinite number of statistical moments. The approach used in this study is to evaluate a finite number of statistical moments and assume certain functions for f_1 and f_2. It is reasonable to approximate travel time, τ, with a lognormal distribution and transverse displacement, η, as a normal distribution (Bellin et al., 1994; Cvetkovic et al., 1996). Based on this assumption, the PDFs can be evaluated from the first two moments of $\tau(x;\mathbf{a})$ and $\boldsymbol{\eta}(x;\mathbf{a})$ as well as their joint moments. Although this method may be valid for any dimensionality, for the purpose of simplicity and illustration, we will focus on transport in 2-D and show how to estimate the moments of $\tau(x;\mathbf{a})$ and $\eta(x;\mathbf{a})$.

In the Lagrangian frame, $\tau(x;\mathbf{a})$ and $\eta(x;\mathbf{a})$ can be related to the velocity field through (Andricevic and

Cvetkovic, 1998; Zhang et al., 2000)

$$\frac{\mathrm{d}\tau}{\mathrm{d}x} = \frac{1}{V_1(x,\eta)}, \qquad \frac{\mathrm{d}\eta}{\mathrm{d}x} = \frac{V_2(x,\eta)}{V_1(x,\eta)} \tag{9}$$

or

$$\tau(x=L;\mathbf{a}) = \int_{a_x}^{L} \frac{\mathrm{d}x}{V_1[x,\eta(x;\mathbf{a})]},$$
$$\eta(x=L;\mathbf{a}) = \int_{a_x}^{L} \frac{V_2[x,\eta(x;\mathbf{a})]}{V_1[x,\eta(x;\mathbf{a})]}\mathrm{d}x \tag{10}$$

where $V_i(x,\eta)$ $(i=1,2)$ is the Lagrangian velocity. Since the Eulerian velocity $\mathbf{V}(x,y)$ is a random variable, so are the Lagrangian velocity $\mathbf{V}(x,\eta)$, the travel time $\tau(x;\mathbf{a})$, and the transverse displacement $\eta(x;\mathbf{a})$. We decompose the Eulerian velocity as $\mathbf{V}(x,y) = \mathbf{U}(x,y) + \mathbf{u}(x,y)$, where $\mathbf{U}$ is the ensemble mean velocity, and $\mathbf{u}$ is a zero-mean velocity fluctuation. For the Lagrangian velocity $\mathrm{V}[x,\eta(x;\mathbf{a})]$, both the particle transverse position η and the velocity $\mathbf{V}$ at this location are random variables. Zhang et al. (2000) expanded the Lagrangian velocity around its mean path $[x,\langle\eta(x;\mathbf{a})\rangle]$ in a Taylor series,

$$V_i(x,\eta) = U_i(x,\langle\eta\rangle) + u_i(x,\langle\eta\rangle) + \eta'\frac{\partial U_i(x,\eta)}{\partial\eta}\bigg|_{\eta=\langle\eta\rangle} + \cdots \quad (i=1,2) \tag{11}$$

where $\eta' = \eta - \langle\eta\rangle$ with $\langle\eta'\rangle \equiv 0$. It should be noted that the mean velocity in the nonstationary field is generally not constant. Substituting Eq. (11) in Eq. (10), one has

$$\tau(L;\mathbf{a}) = \int_{a_x}^{L} \frac{1}{U_1(x,\langle\eta\rangle)}\left[1 - \frac{u_1(x,\langle\eta\rangle)}{U_1(x,\langle\eta\rangle)} - \frac{\eta'}{U_1(x,\langle\eta\rangle)}\frac{\partial U_1(x,\eta)}{\partial\eta}\bigg|_{\eta=\langle\eta\rangle} + \cdots\right]\mathrm{d}x \tag{12}$$

and

$$\eta(x=L;\mathbf{a}) = \int_{a_x}^{L} \frac{1}{U_1(x,\langle\eta\rangle)}[U_2(x,\langle\eta\rangle) + u_2(x,\langle\eta\rangle) - \frac{U_2(x,\langle\eta\rangle)}{U_1(x,\langle\eta\rangle)}u_1(x,\langle\eta\rangle) + \eta'\frac{\partial U_2(x,\eta)}{\partial\eta}\bigg|_{\eta=\langle\eta\rangle} - \eta'\frac{U_2(x,\langle\eta\rangle)}{U_1(x,\langle\eta\rangle)}\frac{\partial U_1(x,\eta)}{\partial\eta}\bigg|_{\eta=\langle\eta\rangle} + \cdots]\mathrm{d}x \tag{13}$$

With these expressions, Zhang et al. (2000) obtained, to the first-order, the means as well as auto- and cross-covariances of τ and η as

$$\langle\tau(L;\mathbf{a})+\rangle = \int_{a_x}^{L} \frac{\mathrm{d}x}{U_1(x,\langle\eta\rangle)} \tag{14}$$

$$\langle\eta(L;\mathbf{a})\rangle = \int_{a_x}^{L} \frac{U_2(x,\langle\eta\rangle)}{U_1(x,\langle\eta\rangle)}\mathrm{d}x \tag{15}$$

$$\sigma_{\tau_1\tau_2}(L,\mathbf{a};L,\mathbf{b}) = \int_{a_x}^{L}\int_{b_x}^{L} \frac{\mathrm{d}x_1\mathrm{d}x_2}{U_1^2(x_1,\langle\eta_1\rangle)U_1^2(x_2,\langle\eta_2\rangle)} \times[\langle u_1(x_1,\langle\eta_1\rangle)u_1(x_2,\langle\eta_2\rangle)\rangle + b_1(x_1,\langle\eta_1\rangle)\langle u_1(x_2,\langle\eta_2\rangle)\eta_1'\rangle + b_1(x_2,\langle\eta_2\rangle)\langle u_1(x_1,\langle\eta_1\rangle)\eta_2'\rangle + b_1(x_1,\langle\eta_1\rangle)b_1(x_2,\langle\eta_2\rangle)\langle\eta_1'\eta_2'\rangle] \tag{16}$$

$$\sigma_{\eta_1\eta_2}(L,\mathbf{a};L,\mathbf{b}) = \frac{1}{U_1^2(L,\langle\eta_1\rangle)U_1^2(L,\langle\eta_2\rangle)}\int_{a_x}^{L}\int_{b_x}^{L}\mathrm{d}x_1\,\mathrm{d}x_2[\langle u_2(x_1,\langle\eta(x_1)\rangle)u_2(x_2,\langle\eta(x_2)\rangle)\rangle + a_1(x_1,\langle\eta(x_1)\rangle)a_1(x_2,\langle\eta(x_2)\rangle)\langle u_1(x_1,\langle\eta(x_1)\rangle) \times u_1(x_2,\langle\eta(x_2)\rangle)\rangle - a_1(x_1,\langle\eta(x_1)\rangle)\langle u_1(x_1,\langle\eta(x_1)\rangle)u_2(x_2,\langle\eta(x_2)\rangle)\rangle - a_1(x_2,\langle\eta_1(x_2)\rangle)\langle u_1(x_2,\langle\eta(x_2)\rangle)u_2(x_1,\langle\eta(x_1)\rangle)\rangle] \tag{17}$$

$$\langle\tau_1'(x_1;\mathbf{a})\eta_2'(x_2;\mathbf{b})\rangle = -\int_{a_x}^{x_1}\frac{1}{U_1^2(\chi,\langle\eta(\chi;\mathbf{a})\rangle)}[\langle u_1(\chi,\langle\eta(\chi;\mathbf{a})\rangle)\eta_2'(x_2;\mathbf{b})\rangle + b_1(\chi,\langle\eta(\chi;\mathbf{a})\rangle)\langle\eta_1'(\chi;\mathbf{a})\eta_2'(x_2;\mathbf{b})\rangle]\mathrm{d}\chi \tag{18}$$

where $b_1(x,\langle\eta\rangle) = \{[\partial U_1(x,y)]/\partial y\}\big|_{y=\langle\eta\rangle}$ and $a_1(x,\langle\eta(x)\rangle) = U_2(x,\langle\eta(x)\rangle)/U_1(x,\langle\eta(x)\rangle)$. We can obtain $\sigma_\tau^2(L,\mathbf{a})$ and $\sigma_\eta^2(L,\mathbf{a})$ by letting $\mathbf{b}=\mathbf{a}$ in Eqs. (16) and (17). As pointed out by Zhang et al. (2000), these expressions are derived under the condition that the coefficient of variation of velocity is smaller than one. This condition may be satisfied for many

practical subsurface flows where the variance of log hydraulic conductivity is moderately large.

If τ and η obey lognormal and normal distributions, respectively, their joint PDF for one particle can be expressed as (Zhang et al., 2000)

$$f_1[\tau(x;\mathbf{a}),\eta(x;\mathbf{a})] = \frac{1}{2\pi\tau\sigma_\eta(x;\mathbf{a})\sigma_{\ln\tau}(x;\mathbf{a})\sqrt{1-r^2}} \exp\left\{-\frac{1}{2(1-r^2)}\left[\frac{(\eta-\langle\eta(x;\mathbf{a})\rangle)^2}{\sigma_\eta^2} - 2r\frac{(\eta-\langle\eta(x;\mathbf{a})\rangle)(\ln\tau-\langle\ln\tau(x;\mathbf{a})\rangle)}{\sigma_\eta(x;\mathbf{a})\sigma_{\ln\tau}(x;\mathbf{a})} + \frac{(\ln\tau-\langle\ln\tau(x;\mathbf{a})\rangle)^2}{\sigma_{\ln\tau}^2(x;\mathbf{a})}\right]\right\} \quad (19)$$

where $\sigma_{\ln\tau}^2(x;\mathbf{a}) = \ln[\sigma_\tau^2(x;\mathbf{a}) + \langle\tau(x;\mathbf{a})\rangle^2] - 2\ln\langle\tau(x;\mathbf{a})\rangle$, $\langle\ln\tau(x;\mathbf{a})\rangle = 2\ln\langle\tau(x;\mathbf{a})\rangle - \frac{1}{2}\ln[\sigma_\tau^2(x;\mathbf{a}) + \langle\tau(x;\mathbf{a})\rangle^2]$, and $r = \langle\tau'(x;\mathbf{a})\eta'(x;\mathbf{a})\rangle/[\sigma_\eta(x;\mathbf{a})\sigma_{\ln\tau}(x;\mathbf{a})\langle\tau(x;\mathbf{a})\rangle]$.Similarly, the joint two-particle PDF of (τ_1,η_1) and (τ_2,η_2) can be expressed as (Zhang et al., 2000)

$$f_2[\tau_1(x;\mathbf{a}),\eta_1(x;\mathbf{a});\tau_2(x;\mathbf{b}),\eta_2(x;\mathbf{b})] = \frac{1}{(2\pi)^2\tau_1\tau_2|\Sigma|^{1/2}}\exp\left\{-\frac{1}{2}\mathrm{X}^T\Sigma^{-1}\mathrm{X}\right\} \quad (20)$$

where $\mathbf{X} = [(\ln\tau_1 - \langle\ln\tau_1\rangle),(\eta_1-\langle\eta_1\rangle),(\ln\tau_2-\langle\ln\tau_2\rangle),(\eta_2-\langle\eta_2\rangle)]^T$ and Σ is the covariance matrix given as

$$\Sigma = \begin{pmatrix} \sigma_{\ln\tau_1}^2 & \sigma_{\ln\tau_1\eta_1} & \sigma_{\ln\tau_1\ln\tau_2} & \sigma_{\ln\tau_1\eta_2} \\ \sigma_{\ln\tau_1\eta_1} & \sigma_{\eta_1}^2 & \sigma_{\ln\tau_2\eta_1} & \sigma_{\eta_1\eta_2} \\ \sigma_{\ln\tau_1\ln\tau_2} & \sigma_{\ln\tau_2\eta_1} & \sigma_{\ln\tau_2}^2 & \sigma_{\ln\tau_2\eta_2} \\ \sigma_{\ln\tau_1\eta_2} & \sigma_{\eta_1\eta_2} & \sigma_{\ln\tau_2\eta_2} & \sigma_{\eta_2}^2 \end{pmatrix} \quad (21)$$

where $\langle\ln\tau_i\rangle = 2\ln\langle\tau_i\rangle - \frac{1}{2}\ln[\sigma_{\tau_i}^2 + \langle\tau_i\rangle^2]$, $\sigma_{\ln\tau_i}^2 = \ln[\sigma_{\tau_i}^2 + \langle\tau_i\rangle^2] - 2\ln\langle\tau_i\rangle$, $\sigma_{\ln\tau_i\eta_j} = \langle\tau_i'\eta_j'\rangle/\langle\tau_i\rangle$, and $\sigma_{\ln\tau_i\ln\tau_j} = \ln[\langle\tau_i\rangle\langle\tau_j\rangle + \langle\tau_i'\tau_j'\rangle] - \ln[\langle\tau_i\rangle\langle\tau_j\rangle]$.

As shown in the above, the various $\ln\tau$ and η moments in Eqs. (19)–(21) can all be expressed with the raw moments of τ and η, which, in turn, are related to the velocity field. In Section 4, we will utilize a perturbation moment method to relate the flow with the hydraulic conductivity and hydraulic boundary conditions (Zhang, 1998; Zhang and Winter, 1999).

4. Spatial moments of velocity covariance

The steady-state flow in a saturated medium satisfies the following continuity equation and Darcy's law

$$\nabla\cdot\mathbf{V}(\mathbf{x}) = 0 \quad (22)$$

$$V_i(\mathbf{x}) = -\frac{K(\mathbf{x})}{n}\frac{\partial h(\mathbf{x})}{\partial x_i} \quad (23)$$

subject to boundary conditions

$$h(\mathbf{x}) = H(\mathbf{x}) \quad x\in\Gamma_D \quad (24)$$

$$\mathbf{V}(\mathbf{x})\cdot\boldsymbol{\gamma}(\mathbf{x}) = \Omega(\mathbf{x}) \quad x\in\Gamma_N \quad (25)$$

where $h(\mathbf{x})$ is hydraulic head, $K(\mathbf{x})$ is hydraulic conductivity (assumed to be isotropic locally), n is the porosity which is assumed to be constant, $H(\mathbf{x})$ is prescribed head on Dirichlet boundary segments Γ_N, $\Omega(\mathbf{x})$ is prescribed flux across Neumann boundary segments Γ_N, and $\boldsymbol{\gamma}(\mathbf{x})$ is an outward unit vector normal to the boundary. In this study, $H(\mathbf{x})$ is assumed to be deterministic and $\Omega(\mathbf{x})$ are assumed to be zero (no flow boundary).

Substituting Eq. (23) into Eq. (22) and utilizing $Y(x) = \ln K(x)$ yields

$$\frac{\partial^2 h(\mathrm{x})}{\partial x_i^2} + \frac{\partial Y(\mathrm{x})}{\partial x_i}\frac{\partial h(\mathrm{x})}{\partial x_i} = 0 \quad (26)$$

Summation for repeated indices is implied. In this study, $Y(\mathbf{x})$ is assumed to be a random variable and is thus decomposed as $Y(\mathbf{x}) = \langle Y(\mathbf{x})\rangle + Y'(\mathbf{x})$, where $\langle Y(\mathbf{x})\rangle$ is the mean log hydraulic conductivity and $Y'(\mathbf{x})$ is the zero-mean fluctuation. In turn, h and V are also random. Since the randomness of h depends on that of Y, one may expand $h(\mathbf{x})$ as

$$h(\mathrm{x}) = h^{(0)}(\mathrm{x}) + h^{(1)}(\mathrm{x}) + h^{(2)}(\mathrm{x}) + \cdots \quad (27)$$

where $h^{(n)}(\mathrm{x}) = O(\sigma_Y^n)$ and σ_Y is the standard deviation of Y. By substituting Eq. (27) into Eq. (26) and collecting terms at separate order, one can obtain the following equations governing the first two

moments involving head (Zhang, 2001),

$$\frac{\partial^2 h^{(0)}(\mathbf{x})}{\partial x_i^2} + \frac{\partial \langle Y(\mathbf{x})\rangle}{\partial x_i}\frac{\partial h^{(0)}(\mathbf{x})}{\partial x_i} = 0 \tag{28a}$$

$$h^{(0)}(\mathbf{x}) = H(\mathbf{x}) \quad \mathbf{x} \in \Gamma_D \tag{28b}$$

$$\gamma_i(\mathbf{x})\frac{\partial h^{(0)}(\mathbf{x})}{\partial x_i} = 0 \quad \mathrm{x} \in \Gamma_N \tag{28c}$$

$$\frac{\partial^2 \langle h^{(2)}(\mathbf{x})\rangle}{\partial x_i^2} + \frac{\partial \langle Y(\mathbf{x})\rangle}{\partial x_i}\frac{\partial \langle h^{(2)}(\mathbf{x})\rangle}{\partial x_i} = -\frac{\partial}{\partial x_i}\frac{\partial}{\partial \chi_i}[C_{Yh}(\mathbf{x},\boldsymbol{\chi})]|_{\mathbf{x}=\boldsymbol{\chi}} \tag{29a}$$

$$\langle h^{(2)}(\mathbf{x})\rangle = 0 \quad \mathbf{x} \in \Gamma_D \tag{29b}$$

$$\gamma_i(\mathbf{x})\frac{\partial \langle h^{(2)}(\mathbf{x})\rangle}{\partial x_i} = 0 \quad \mathbf{x} \in \Gamma_N \tag{29c}$$

$$\frac{\partial^2 C_h(\mathbf{x},\chi)}{\partial x_i^2} + \frac{\partial \langle Y(\mathbf{x})\rangle}{\partial x_i}\frac{\partial C_h(\mathbf{x},\chi)}{\partial x_i} = J_i(\mathbf{x})\frac{\partial C_{Yh}(\mathbf{x},\boldsymbol{\chi})}{\partial x_i} \tag{30a}$$

$$C_h(\mathbf{x},\boldsymbol{\chi}) = 0 \quad \mathrm{x} \in \Gamma_D \tag{30b}$$

$$\gamma_i(\mathbf{x})\frac{\partial C_h(\mathbf{x},\boldsymbol{\chi})}{\partial x_i} = 0 \quad \mathrm{x} \in \Gamma_N \tag{30c}$$

$$\frac{\partial^2 C_{Yh}(\mathbf{x},\chi)}{\partial \chi_i^2} + \frac{\partial \langle Y(\boldsymbol{\chi})\rangle}{\partial \chi_i}\frac{\partial C_{Yh}(\mathbf{x},\chi)}{\partial \chi_i} = J_i(\boldsymbol{\chi})\frac{\partial C_Y(\mathbf{x},\boldsymbol{\chi})}{\partial \chi_i} \tag{31a}$$

$$C_{Yh}(\mathbf{x},\boldsymbol{\chi}) = 0 \quad \boldsymbol{\chi} \in \Gamma_D \tag{31b}$$

$$\gamma_i(\mathbf{x})\frac{\partial C_{Yh}(\mathbf{x},\boldsymbol{\chi})}{\partial \chi_i} = 0 \quad \boldsymbol{\chi} \in \Gamma_N \tag{31c}$$

In the above, $h^{(0)}$ is the zeroth-order mean head, $\langle h^{(2)}\rangle$ is the second-order mean head correction term, $J_i = -\partial h^{(0)}/\partial x_i$ is the negative of the (zeroth-order) mean hydraulic head gradient, $C_{Yh} = \langle Y'(\mathbf{x})h^{(1)}(\boldsymbol{\chi})\rangle$ is the cross-covariance between log hydraulic conductivity and head, and $C_h = \langle h^{(1)}(\mathbf{x})h^{(1)}(\boldsymbol{\chi})\rangle$ is the head covariance. Since $\langle h^{(1)}\rangle$ (the mean of the first-order correction term) is zero, $\langle h\rangle = h^{(0)}$ to zeroth- or first-order in σ_Y, and $\langle h\rangle = h^{(0)} + \langle h^{(2)}\rangle$ to second order. In the above, the covariances are of second order in σ_Y (or first-order in σ_Y^2).

All terms on the right-hand side of Eq. (31a)–(31c) are known with the solution of $h^{(0)}$ from Eq. (28a)–(28c), hence the equation governing C_{Yh} is deterministic and fully solvable. With C_{Yh}, one can obtain C_h from Eq. (30a)–(30c), and $\langle h^{(2)}\rangle$ from Eq. (29a)–(29c). However, due to the mathematical complexity, it is essentially impossible to obtain analytical solutions for the problem. Zhang (1998) and Zhang and Winter (1999) developed a finite difference scheme for solving the statistical moment equations.

We next show how to derive the statistical moments of the velocity field. The velocity in Eq. (23) can be rewritten as

$$\mathbf{V}(\mathbf{x}) = -\frac{K_G(\mathbf{x})}{n}\left[1 + Y' + \frac{Y'2}{2} + \cdots\right]\nabla \times [h^{(0)} + h^{(1)} + h^{(2)} + \cdots] \tag{32}$$

Collecting terms at separate order, we have up to the second-order

$$\mathbf{V}^{(0)}(\mathbf{x}) = -\frac{K_G(\mathbf{x})}{n}\nabla h^{(0)}(\mathbf{x}) \tag{33}$$

$$\mathbf{V}^{(1)}(\mathbf{x}) = -\frac{K_G(\mathbf{x})}{n}[Y'(\mathbf{x})\nabla h^{(0)}(\mathbf{x}) + \nabla h^{(1)}(\mathbf{x})] \tag{34}$$

$$\mathbf{V}^{(2)}(\mathbf{x}) = -\frac{K_G(\mathbf{x})}{n}[Y'(\mathbf{x})\nabla h^{(1)}(\mathbf{x}) + \frac{Y'2(\mathbf{x})}{2}\nabla h^{(0)}(\mathbf{x}) + \nabla h^{(2)}(\mathbf{x})] \tag{35}$$

It can be shown that the mean velocity is $\langle \mathbf{V}\rangle = \mathbf{V}^{(0)}$ to zeroth- or first-order in σ_Y, $\langle \mathbf{V}\rangle = \mathbf{V}^{(0)} + \langle \mathbf{V}^{(2)}\rangle$ to second order, and the velocity fluctuation is $\mathbf{V}' = \mathbf{V}^{(1)}$ to first-order. Therefore, the velocity covariance is given as

$$C_{v_{ij}}(\mathbf{x},\boldsymbol{\chi}) = \frac{K_G(\mathbf{x})K_G(\boldsymbol{\chi})}{n^2}\left[J_i(\mathbf{x})J_j(\boldsymbol{\chi})C_Y(\mathbf{x},\boldsymbol{\chi}) - J_i(\mathbf{x})\frac{\partial C_{Yh}(\mathbf{x},\boldsymbol{\chi})}{\partial \chi_j} - J_j(\boldsymbol{\chi})\frac{\partial C_{Yh}(\boldsymbol{\chi},\mathbf{x})}{\partial x_i} + \frac{\partial^2 C_h(\mathbf{x},\boldsymbol{\chi})}{\partial x_i \partial \chi_j}\right] \tag{36}$$

The second-order correction term to the velocity is obtained from Eq. (35) as

$$\langle V_i^{(2)}(\mathbf{x})\rangle = -\frac{K_G(\mathbf{x})}{n}\left[\frac{\partial C_{Yh}(\boldsymbol{\chi};\mathbf{x})}{\partial x_i}\Big|_{\boldsymbol{\chi}=\mathbf{x}} - \frac{J_i(\mathbf{x})}{2}\sigma_Y^2(\mathbf{x}) + \frac{\partial}{\partial x_i}\langle h^{(2)}(\mathbf{x})\rangle\right] \tag{37}$$

All the terms on the right-hand side of Eqs. (36) and (37) are known, therefore $C_{v_{ij}}$ and $\langle \mathbf{V}_i^{(2)} \rangle$ can be obtained with the availability of the moments of head.

5. Synthetic case study

In previous sections, the theoretical framework has been developed for the estimation of solute flux. The required data for the calculation are the statistical moments of the conductivity field, solute initial distribution, and hydraulic boundary conditions. In this section, we will use several case studies to show the effects of these factors on solute transport processes.

5.1. Nonstationarity of conductivity field

The spatial nonstationarity of groundwater flow may be generated from the presence of multi-scale and nonstationary medium features (e.g. distinct geologic layers, zones or faces), the presence of finite boundaries, and/or the fluid pumping and injecting. Here, we consider flow nonstationarity stemming from the combined effects of the nonstationarity in the hydraulic conductivity and the finite boundary. The nonstationarity in the Y field may manifest in two ways: the mean $\langle Y \rangle$ may vary spatially, and the two-point covariance $C_Y(x, \chi)$ may depend on the actual locations of x and χ rather than only their separation distance. In this subsection, we consider the case that the log hydraulic conductivity consists of a nonYucca Mountain, Nevadaconstant mean and a stationary fluctuation. That is to say, the mean varies spatially and the two-point covariance only depends on the relative distance. Later, we will study the more general case that the two-point covariance depends on the actual locations of the two points in Section 5.4. More detailed discussion on multi-scale and nonstationary random fields is recently given by Zhang et al. (2000).

Although the covariance of Y may take any admissible form, here we consider, for simplicity, only the exponential form

$$C_Y(\mathbf{x} - \boldsymbol{\chi}) = \sigma_Y^2 \exp\{ - [(x_i - \chi_i)^2/\lambda_i^2]^{1/2} \} \qquad (38)$$

where σ_Y^2 is the variance and $\lambda_i (i = 1, 2)$ is the correlation scale of Y along the x_i axis. For the sake of simplicity, here we use $\lambda_1 = \lambda_2 = \lambda$.

Fig. 1 is the sketch of a synthetic two-dimensional (2-D) domain of size $11\lambda \times 11\lambda$ (λ is the log-conductivity correlation length). Here, we consider a high (or low) permeability layer in an otherwise stationary permeability field. The layer may be parallel to the x-coordinate (Layer A), perpendicular to the x-coordinate (Layer B), or in a 45° angle to the x-coordinate (Layer C). The mean log hydraulic conductivity within the layer is chosen to be $\langle Y \rangle = 1$ for a high-permeability case, or $\langle Y \rangle = -1$ for a low-permeability case. In both cases, the variance is $\sigma_Y^2 = 1$, and the correlation length is 1 [L]. For the rest of the domain, the variance and correlation length are the same as those for the layer, but the mean log hydraulic conductivity is chosen to be $\langle Y \rangle = 0$ (correspondingly, the geometric mean $K_G = 1[L/T]$). According to the layer's orientation and mean conductivity value, seven different combinations are listed in Table 1. The boundary conditions are specified as follows: constant hydraulic head ($h = 11\lambda$) for the left side ($x = 0$), constant hydraulic head ($h = 0$) for the right side ($x = 11\lambda$), and no flow for the lower ($y = 0$) and upper ($y = 11\lambda$) boundaries.

For Case 1, there is no multi-scale feature in the simulation domain. The flow nonstationarity is resulted only from the finite boundaries. The results of this case are used as references for the other

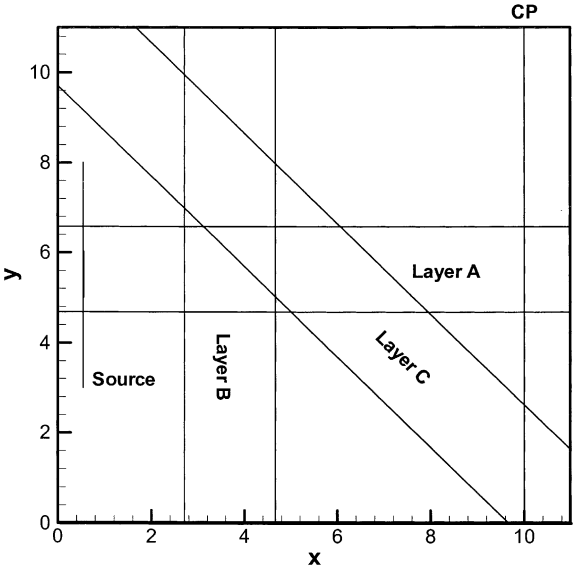

Fig. 1. Sketch of the study domain as well as the locations of source, control plane (CP), and high- (or low)-permeability layers.

Table 1
Seven cases of the hydraulic conductivity field

Case	Layer	⟨Y⟩
1	None	0
2	Layer A (parallel to x direction)	1
3	Layer B (perpendicular to x direction)	1
4	Layer C (inclined to x direction)	1
5	Layer A (parallel to x direction)	-1
6	Layer B (perpendicular to x direction)	-1
7	Layer C (inclined to x direction)	-1

cases. In Cases 2–4, the domain involves a high-permeability layer A, B and C, respectively; in Cases 5–7, the domain involves a low-permeability layer A, B and C, respectively. In all of these cases, the line source with unit mass is of size $H = 1\lambda$ centered at the point $(0.5\lambda, 5.5\lambda)$, and the control plane (CP) is located at $x = 10\lambda$.

The groundwater flow distributions for the seven cases have been calculated. For the purpose of illustration and brevity, we use the results of Case 4, shown in Fig. 2, to exhibit the nonstationary flow domain. It is seen from the figure that the existence of high-permeability layer C results in a significant change of mean flow in both direction and magnitude, which leads to flow nonstationarity

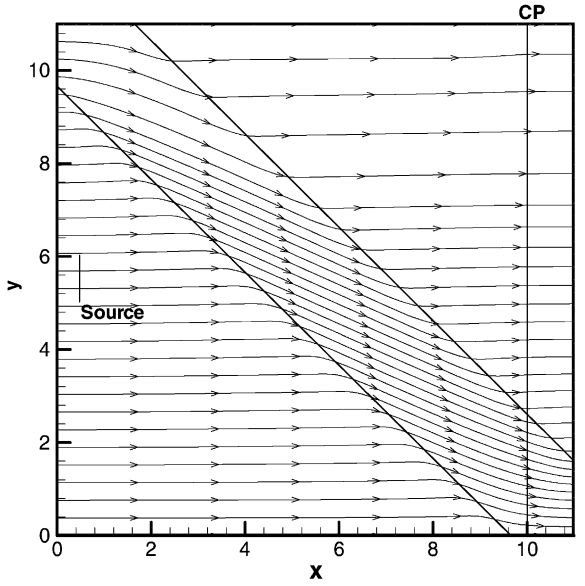

Fig. 2. Illustration of the mean flow field with the inclined high-permeability layer C.

in the domain. Though not shown, the (co)variance of the velocity field is also strongly location dependent and thus nonstationary.

Fig. 3 shows the transport results of Cases 1–4. The figure reveals the effect of a high-permeability layer with various orientations on solute flux. Fig. 3(a) and (b) are the profiles of the mean total solute flux, $\langle Q \rangle$, and the associated uncertainty, σ_Q, across the CP as a function of time, respectively. In comparison of the four mean breakthrough curves, it is apparent that the inclusion of a high-permeability layer would generally render an earlier solute arrival (i.e. faster advection) and a higher peak for $\langle Q \rangle$ (i.e. less dispersion). More specifically, the mean solute transport is the fastest in Case 2 since the solute moves only in the high-permeability layer (fast channel), which results in an early breakthrough with the largest peak. The breakthrough curve reaches its peak value and then drops quickly to zero. On the other hand, for Case 1, the mean solute movement is much slower in the domain without the high-permeability layer. It results in a later breakthrough curve with the smallest peak value. The curve spreads widely and has a long tail. The results of Cases 3 and 4 are between those of Cases 1 and 2. It is also shown that the mean solute transport is faster in Case 4 than that in Case 3 since the high-permeability layer in Case 4 is more inclined to the solute transport direction. The profiles of the standard deviation σ_Q in Fig. 3b are consistent with the results of $\langle Q \rangle$, where larger $\langle Q \rangle$ corresponds to the larger σ_Q. Further, σ_Q is generally larger than $\langle Q \rangle$ for the cases studied with the specific σ_Y value and source dimension.

Fig. 3(c) and (d) are the profiles of the mean solute flux $\langle q \rangle$ and the associated standard deviation σ_q for the plume at the center point of CP (i.e. at the point $(10\lambda, 5.5\lambda)$) as a function of time, respectively. It is apparent that a high-permeability layer has a similar effect on $\langle q \rangle$ and σ_q as on $\langle Q \rangle$ and σ_Q. The difference is that the solute plume in Case 4, instead of Case 1, has the smallest peak. This phenomenon is due to the change of mean solute transport direction resulting from the orientation of the high-permeability layer. One may imagine that the breakthrough curve of $\langle q \rangle$ at the center of the plume (instead at the center of CP) will have the same characteristics as that of $\langle Q \rangle$ for the four cases. In Fig. 3(e) and (f), we present the $\langle q \rangle$ and σ_q profiles, respectively, as a function of transverse

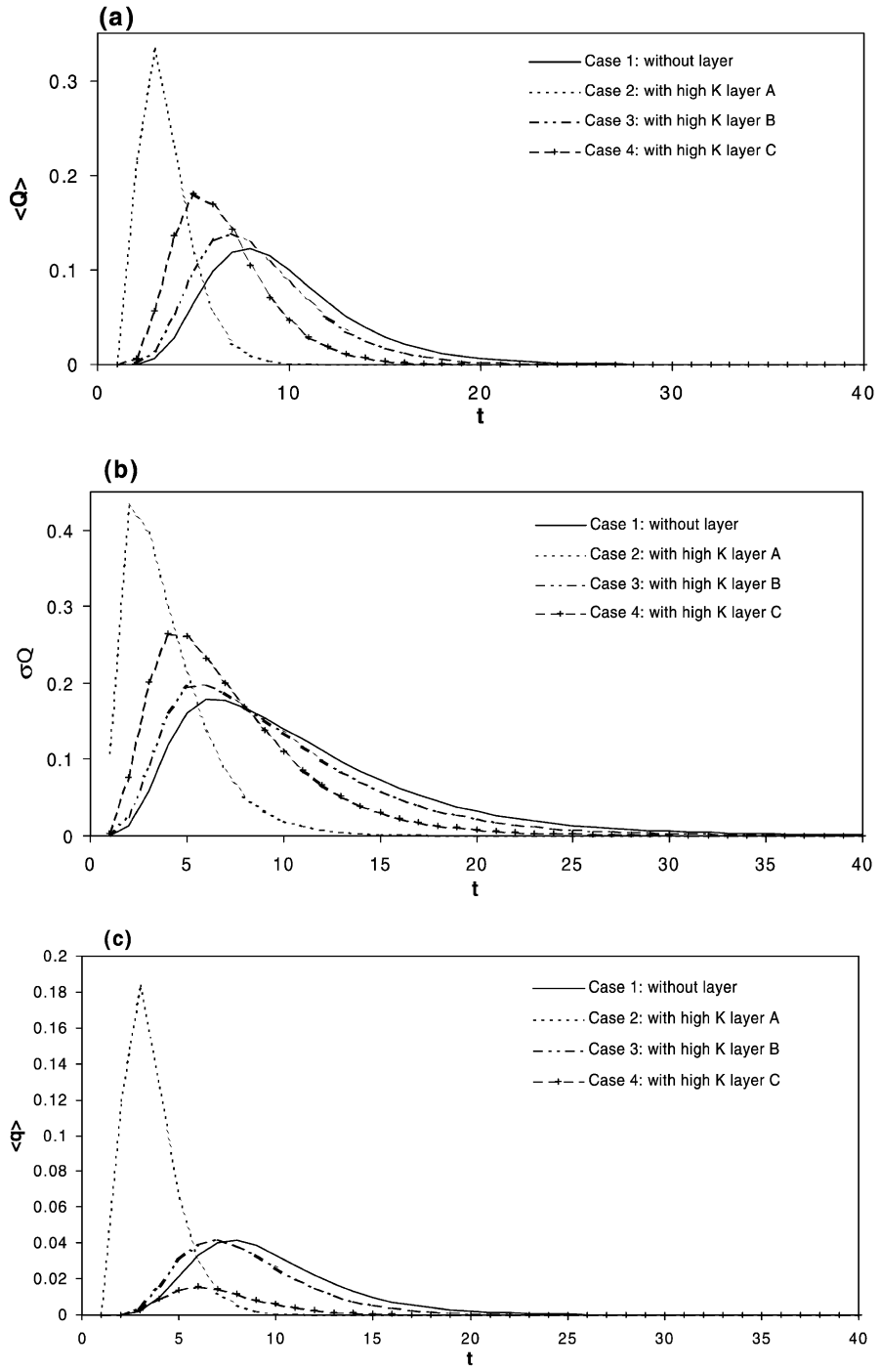

Fig. 3. (a) Expected value $\langle Q \rangle$ and (b) standard deviation σ_Q of total solute flux, (c), (e) expected value $\langle q \rangle$, and (d), (f) standard deviation σ_q of point solute flux across the control plane at $x = 10\lambda$ (a, b, c and d) as a function of time and (e and f) as a function of transverse displacement with various high-permeability layers.

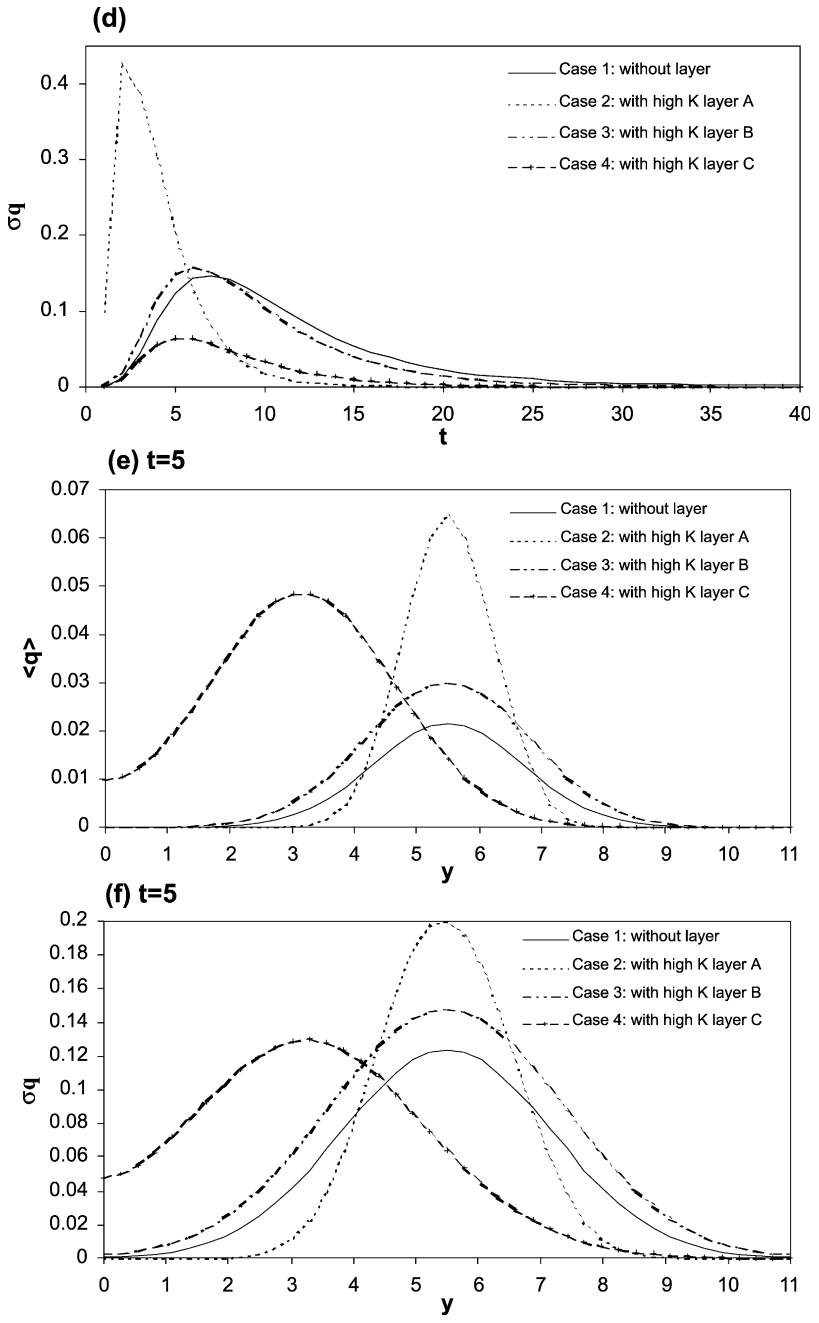

Fig. 3 (*continued*)

location on the CP at $t = 5$. It is seen that both the $\langle q \rangle$ and σ_q have Gaussian-type (single-modal) profiles in the transverse direction. For Case 4, the change of the solute transport direction results in the nonsymmetric distributions of the $\langle q \rangle$ and σ_q in the transverse direction on the CP.

Fig. 4 exhibits the solute flux results of Cases 1, 5, 6, and 7. This figure is the counterpart of Fig. 3, but

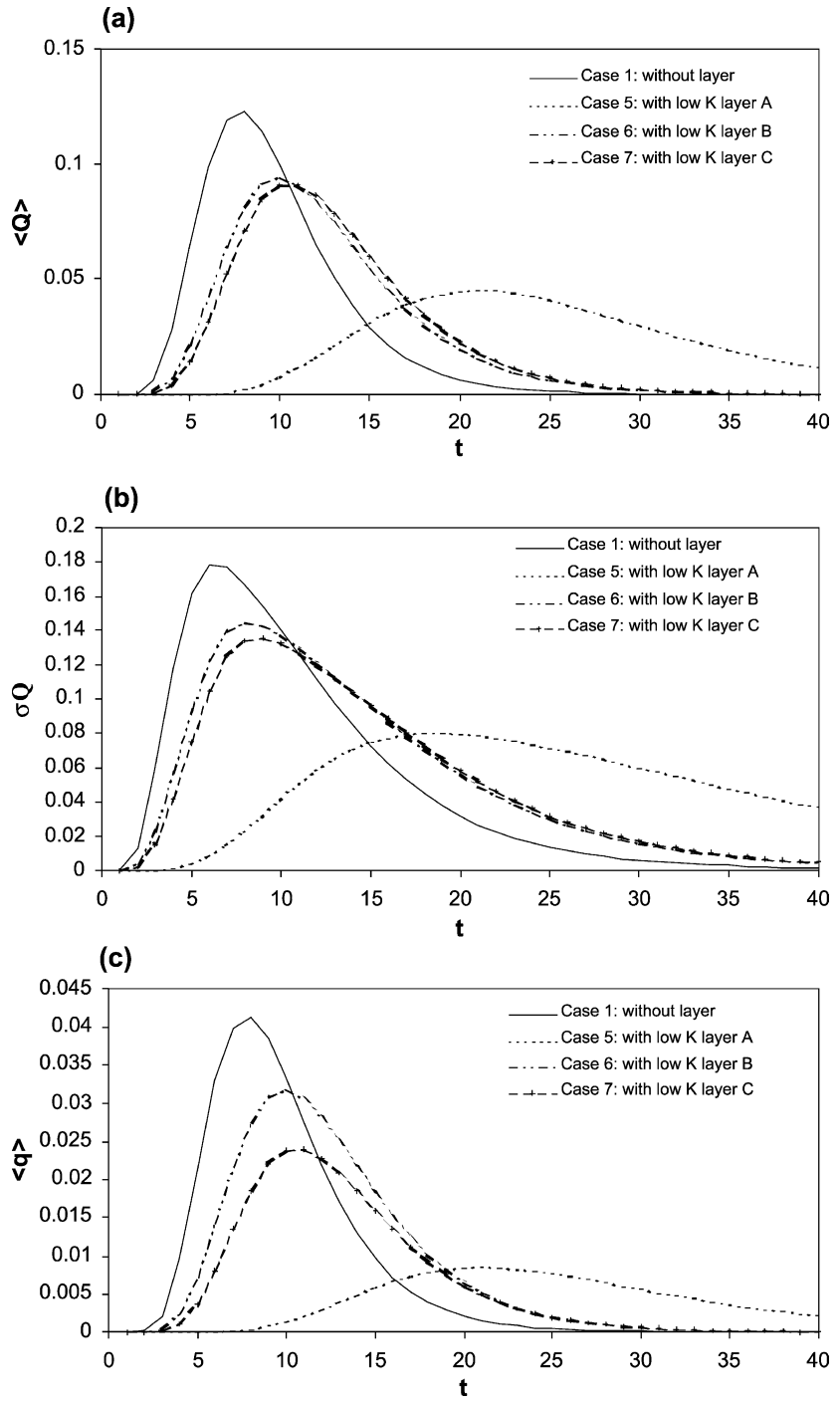

Fig. 4. (a) Expected value $\langle Q \rangle$ and (b) standard deviation σ_Q of total solute flux, (c), (e) expected value $\langle q \rangle$, and (d), (f) standard deviation σ_q of point solute flux across the control plane at $x = 10\lambda$ (a, b, c and d) as a function of time and (e and f) as a function of transverse displacement with various low-permeability layers.

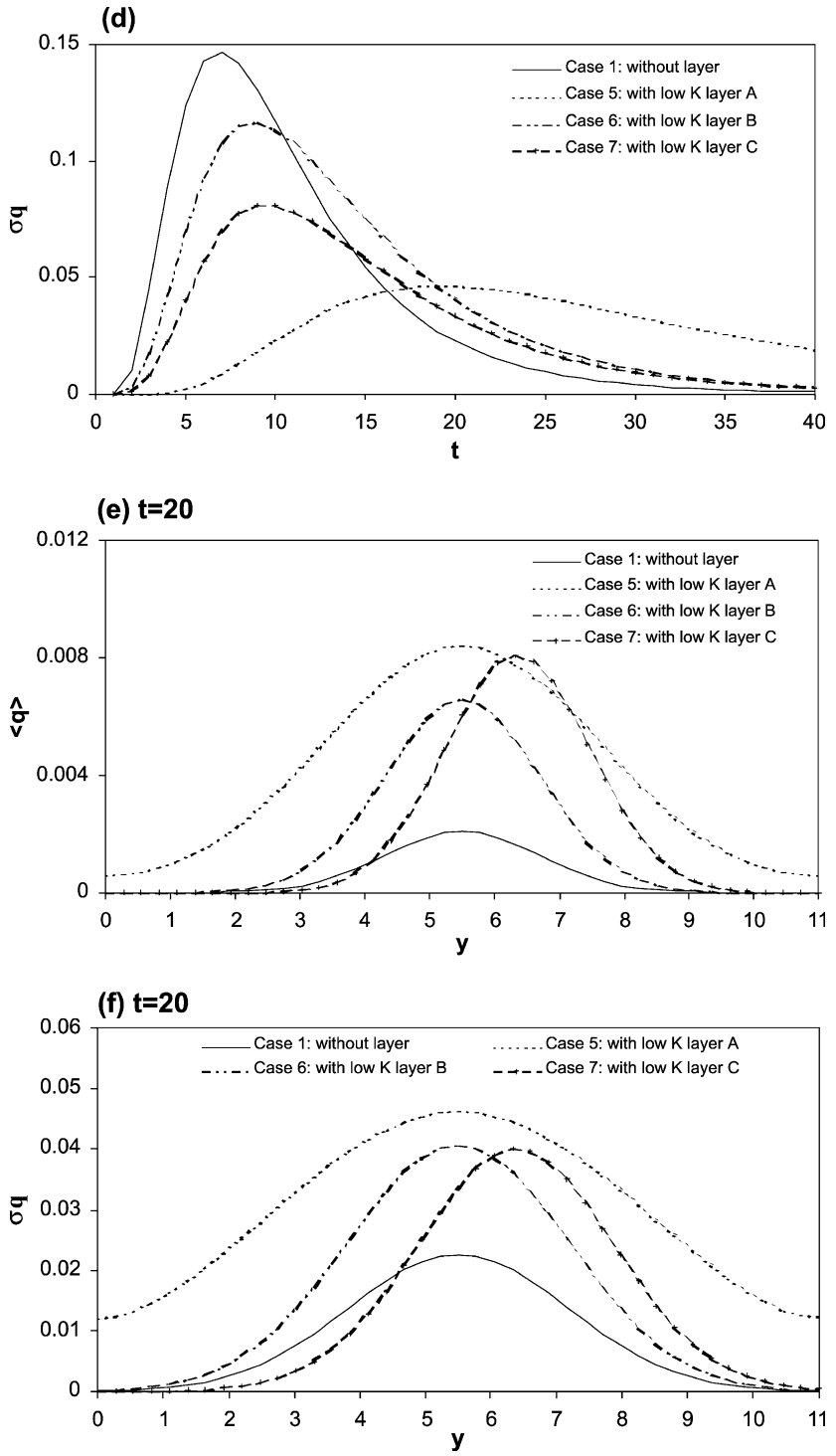

Fig. 4 (*continued*)

with a low-permeability layer. Contrary to the effect of the high layer on solute transport, the existence of the low conductivity layer retards the solute movement, generate more dispersion and decrease the peak values of $\langle Q \rangle$ and $\langle q \rangle$ breakthrough curves. The long tailing is more obvious. The $\langle q \rangle$ profile along the y-direction in the CP is also nonsymmetric, but the curve is skewed in the opposite side in comparison to the case with the high conductivity zone. The existence of low conductivity decreases the σ_Q and σ_q in the longitudinal direction, but increases σ_q in the transverse direction.

5.2. Hydraulic boundary conditions

In this subsection, we will study flow nonstationarity caused by hydraulic boundary conditions, and the influence of this flow nonstationarity on solute flux. The stationary conductivity field shown in Section 5.1 as Case 1 is chosen for this study, so we can focus on the boundary influence. The boundary hydraulic conditions at the top, bottom and right sides are the same as those in Section 5.1, but different on the left side. In Section 5.1, the hydraulic head on the whole left side is fixed at $H = 11\lambda$. Here, we let the hydraulic head decrease linearly from $H = 11\lambda$ at the top to $H = 7\lambda$ at the bottom. The mean flow field in this case is shown in Fig. 5. It is seen that the variation of the hydraulic head on the left boundary results in the change of the mean flow in both magnitude and direction, especially in the vicinity of the boundary. The computed results of solute flux in this flow field are shown in Fig. 6. For the purpose of comparison, the solute flux results of Section 4's Case 1 are also shown in the figure.

Fig. 6(a) presents the profiles of $\langle Q \rangle$ and σ_Q across the CP as a function of time. It is shown that the changed hydraulic head boundary on the left side renders a later solute arrival (i.e. slower advection) and a lower peak for $\langle Q \rangle$ (i.e. greater dispersion). This phenomenon is due to the decrease of the flow velocity and change of flow direction by the variation of the left boundary condition. Fig. 6a also shows that the profile of σ_Q is consistent with that of $\langle Q \rangle$, and the value of σ_Q is generally larger than $\langle Q \rangle$. This result is consistent with what we have found in Section 5.1. Fig. 6b shows the profiles of the $\langle q \rangle$ and the σ_q at the center of the CP as a function of time. It is apparent

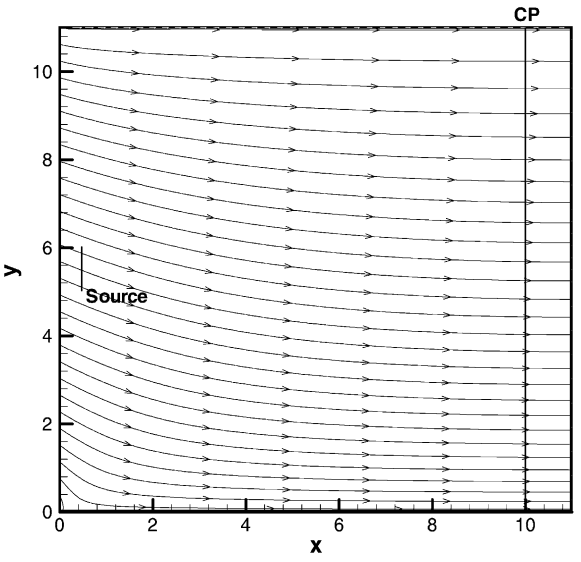

Fig. 5. Illustration of the mean flow field with the linearly decreasing hydraulic head boundary condition.

that the change of the boundary condition significantly affects $\langle q \rangle$ and σ_q. Comparing Fig. 6a and b, one may note (not shown in the figure) that the relative uncertainty of Q, $\sigma_Q/\langle Q \rangle$, is much less than that of q, $\sigma_q/\langle q \rangle$. In Fig. 6c, we present the profiles of $\langle q \rangle$ and σ_q as a function of the transverse location on the CP at $t = 10$. It is shown that the change of boundary leads to the skewed distribution of $\langle q \rangle$ and σ_q, and the decrease of $\langle q \rangle$ and σ_q at the center of the CP, and also the decrease of the relative uncertainty of q.

In summary, the change of boundary conditions leads to the flow nonstationarity in both magnitude and direction, which in turn significantly affects the solute transport processes for solute flux and total solute flux. It is also shown that the method used in this study can capture the hydraulic characteristics caused by the complex boundary conditions and their influence on solute transport.

5.3. Initial plume distribution

In Sections 5.1 and 5.2, the initial plume is chosen to be a unit line with constant density and located at the center of the left boundary. Here, we will study the effects of geometry and density of the initial plume distribution on solute flux. For the purpose of

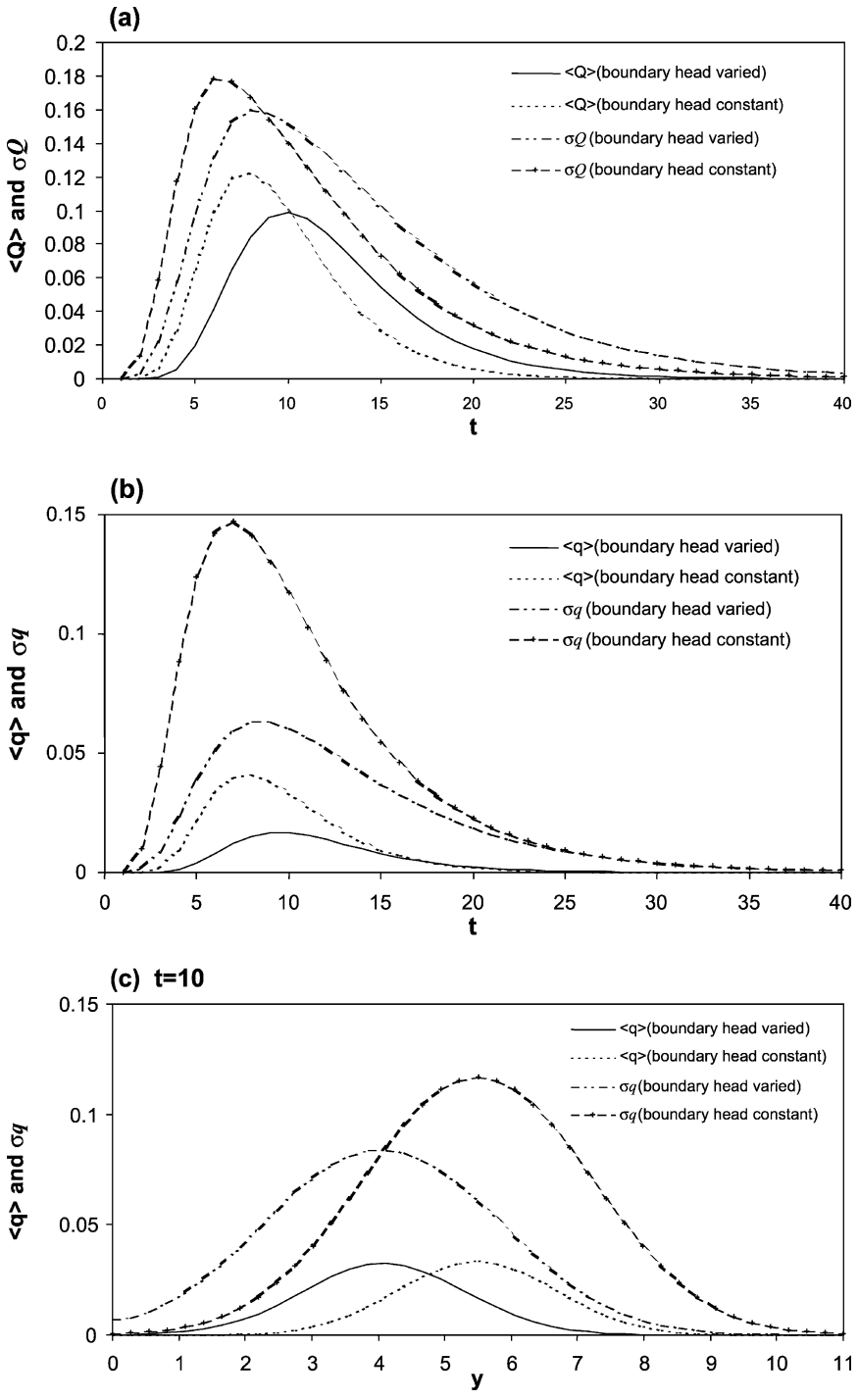

Fig. 6. (a) Expected value $\langle Q \rangle$ and standard deviation σ_Q of total solute flux, (b) expected value $\langle q \rangle$ and standard deviation σ_q of point solute flux across the control plane at $x = 10\lambda$ as a function of time, and (c) as a function of transverse displacement with the linear decreased hydraulic head boundary condition.

comparison, the total mass of the initial plume is fixed as 1 unit in this subsection. The simulation domain is chosen to be the same as that for Case 2 of Section 5.1, the high-permeability layer A in an otherwise statistically homogeneous medium. The boundary condition is the same as that in Section 5.1. In this subsection, three source distributions are examined. In the first two cases, the lengths of the line sources are chosen to be $H = 5\lambda$. The source density is constant for Scenario 1. For Scenario 2, we divide the length into five equivalent pieces, each with 1λ length. The mass density in the three middle pieces are zero, and the solute of unit mass is uniformly distributed at the two end pieces. In Scenario 3, the length of the line source is $H = 1\lambda$ and the density is constant. The line sources in all three cases are all centered at $(0.5\lambda, 5.5\lambda)$.

In Fig. 7a and b, we present the $\langle q \rangle$ and σ_q breakthrough curves, respectively, through the center of the CP (i.e. at point $(10\lambda, 5.5\lambda)$). As shown in the figures, the solute breakthrough curve in Scenario 3 has the highest peak and the earliest arrival in the three cases, because the whole source is within the high-permeability layer. Correspondently, the case also renders the largest σ_q. When the length of the source is $H = 5\lambda$ (Scenarios 1 and 2), in comparison with the constant density source (Scenario 1), the variable density source with mass concentrated at the two ends (Scenario 2) results in the much slower advection and much larger dispersion. It should be noted that source distribution in Scenario 1 leads to the smallest solute flux uncertainty in the three cases, which can be explained as that the larger the source size, the smaller the uncertainty. This result is consistent with relative dispersion theory (Andricevic and Cvetkovic, 1998].

Fig. 7c and d shows the $\langle q \rangle$ and σ_q profiles, respectively, as a function of transverse location on the CP at $t = 5$. It is shown that for Scenarios 1 and 3, both $\langle q \rangle$ and σ_q have Gaussian-type (single-model) profiles in the transverse direction at this early travel time. However, the two profiles for Scenario 2 at the same time have bimodal distributions, which are caused by the two separate sources at the two ends.

Fig. 8 shows the $\langle q \rangle$ and σ_q profiles for Scenario 1 as a function of transverse location on the CP at different times. In the early travel time, both $\langle q \rangle$ and σ_q have Gaussian-type (single-modal) profiles. At

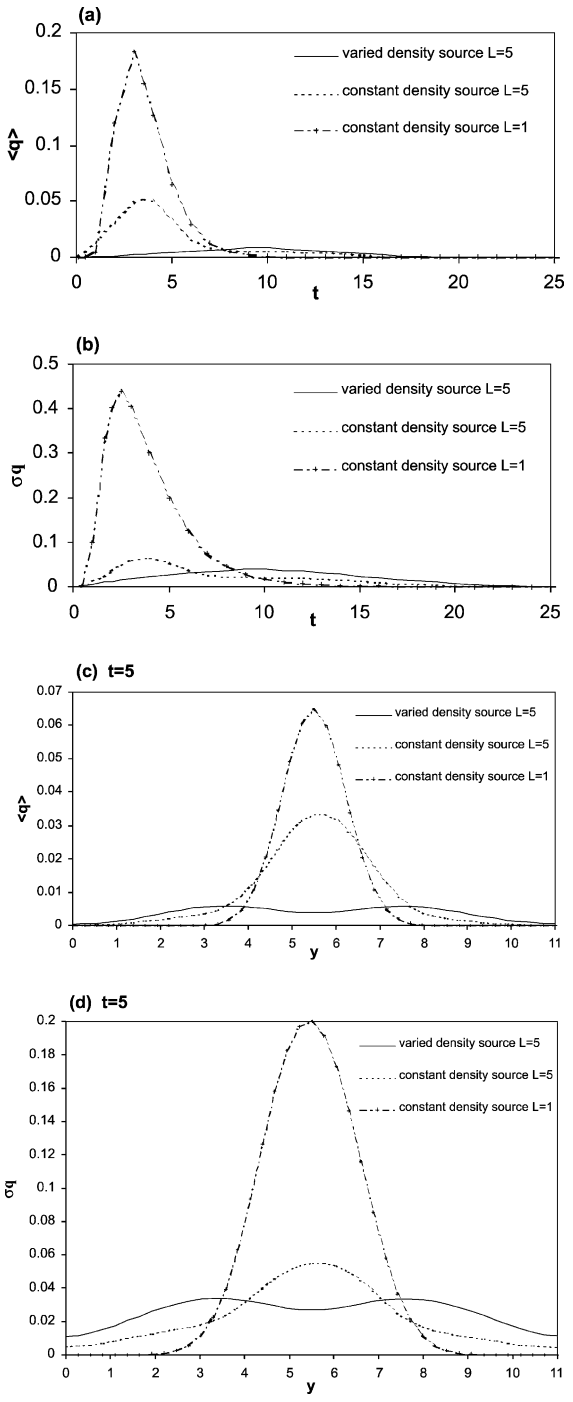

Fig. 7. (a), (c) Expected value $\langle q \rangle$ and (b), (d) standard deviation σ_q of point solute flux across the control plane at $x = 10\lambda$ (a and b) as a function of time and (c and d) as a function of transverse displacement with different source conditions.

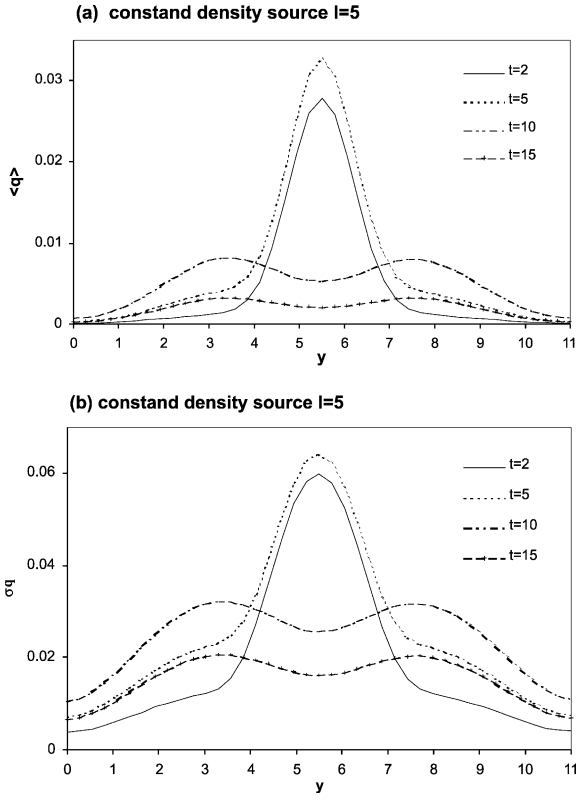

Fig. 8. (a) Expected value $\langle q \rangle$ and (b) standard deviation σ_q of point solute flux due to a constant density source of length 5λ across the control plane at $x = 10\lambda$ as a function of transverse displacement at $t = 2$, 5, 10, and 15 with the high-permeability layer A.

longer travel time, however, the two profiles become bimodal.

5.4. Covariance of hydraulic conductivity

In all the case studies above, we assume the log hydraulic conductivity field consists of a nonconstant mean, but a stationary fluctuation. In the natural environment, two media, even next to each other, may have quite different structures of C_Y. Even if the two media have the same structures, the parameter values, such as the variance and the correlation length, can be quite different. There may be no conductivity correlation between the two media. Of all these issues, the conductivity correlation across the boundary of the two regions is probably the most important one for the extension of the solute transport model from one region to multiple regions.

In this subsection, we examine the effect of the different forms of C_Y across the regional boundaries on the solute transport. The simulation domain, mean conductivity distribution and boundary conditions are chosen to be the same as those in Case 4 of Section 5.1. However, in Section 5.1, the existence of layer C does not influence C_Y, which means that whether the two points, $\mathbf{x}$ and χ, are in the same region or not, the correlation is $C_Y(\mathbf{x}, \boldsymbol{\chi}) = C_Y(\mathbf{x} - \boldsymbol{\chi})$. This case is called universal correlation. In this subsection, we consider another case, called regional correlation, where $C_Y(\mathbf{x}, \boldsymbol{\chi}) = C_Y(\mathbf{x} - \boldsymbol{\chi})$ if $\mathbf{x}$ and χ are in the same region (medium), otherwise $C_Y(\mathbf{x}, \boldsymbol{\chi}) = 0$.

We present the $\langle q \rangle$ and σ_q breakthrough curves through the center point at the CP in Fig. 9a, and their profiles as a function of transverse location on the CP for $t = 5$ in Fig. 9b. It is shown that in comparison with the universal correlation, the regional correlation results in faster advection, less dispersion and larger uncertainty. We can imagine that the influence of the correlation between two media would be more significant if the $\langle Y \rangle$, σ_Y^2 and the structure of C_Y are all different in the two media.

6. Application to Yucca Mountain environmental project

Yucca Mountain is located in the Great Basin about 150 km northwest of Las Vegas, Nevada. The mountain consists of a series of fault-bounded blocks of ash-flow and ash-fall tuffs and a smaller volume of lava deposited between 14 and 11 Ma (million years before present) from a series of calderas located at a few to several tens of kilometers to the north. This location was chosen by the US Department of Energy as a candidate for storing radionuclide wastes. Many numerical studies have been conducted to simulate the potential solute transport process after the radionuclide wastes migrate from the repository to the saturated groundwater (e.g. Zyvoloski et al., 1997). The saturated medium is composed of many layers of different materials. These materials in different layers have quite different physical properties (e.g. hydraulic conductivity). Even within a single layer, significant spatial heterogeneity of hydraulic conductivity has

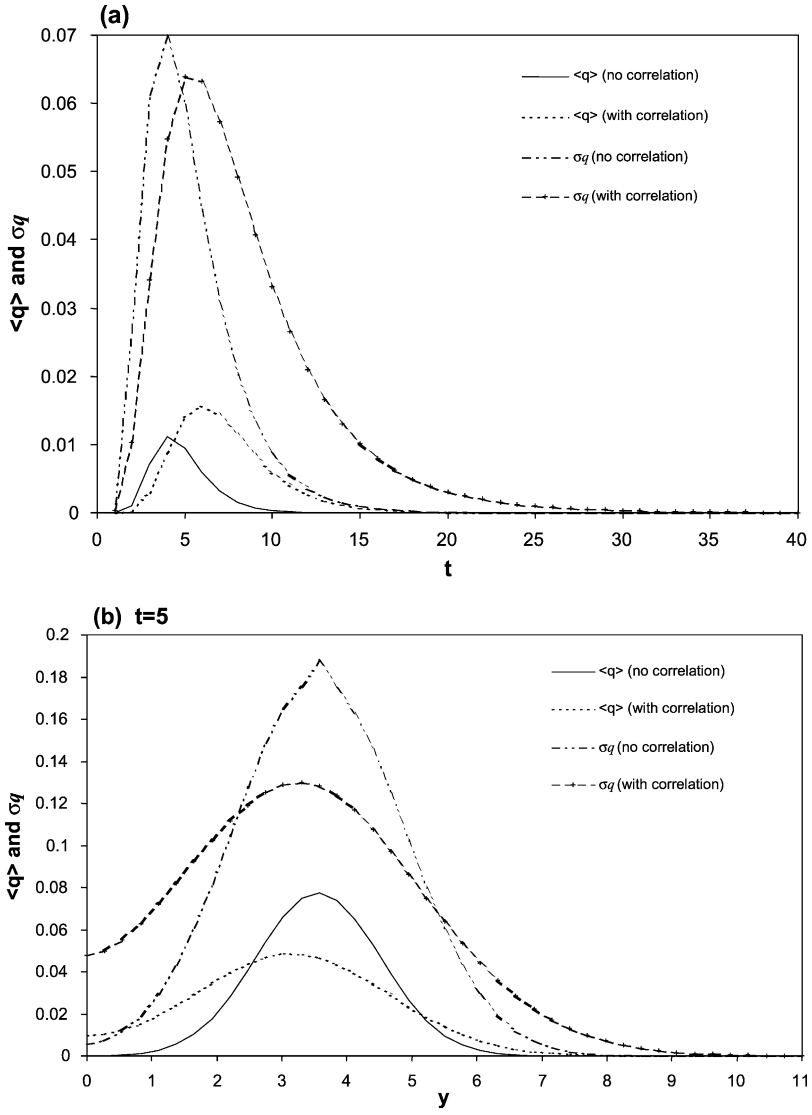

Fig. 9. Expected value $\langle q \rangle$ and standard deviation σ_q of point solute flux across the control plane at $x = 10\lambda$ (a) as a function of time and (b) as a function of transverse displacement with different covariances of log hydraulic conductivity (C_Y) of different permeability medium.

been observed (Shirley et al., 1997). However, owing to the tremendous computational demand of conducting Monte Carlo simulations to study the influence of heterogeneity within each layer on groundwater flow and solute transport, current numerical modeling efforts are limited to the deterministic approach with effective parameter values, such as the mean conductivity and macrodispersivity. This deterministic approach may predict the mean or expected flow and solute transport processes, but it cannot fully address the uncertainties about the expected predictions. Here, we use the moment method to study this issue.

As shown in Fig. 10, the study domain, 5200 m horizontally and 940 m vertically, is a vertical cross section parallel to the mean flow. There are six layers within this domain and the dash lines represent the boundaries of the layers. The mean of the log-conductivity within each layer is shown in the figure. The geostatistical study of the conductivity

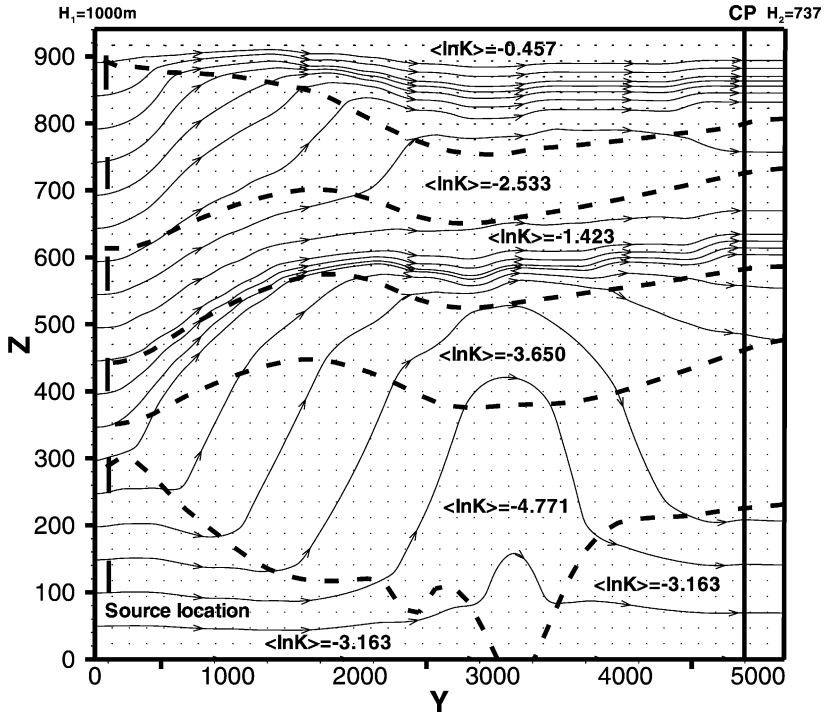

Fig. 10. Sketch of the study domain, the locations of source and CP, and the mean flow field.

distribution within each layer is in progress. For the purpose of illustration, we assume the log-conductivity in every layer has an isotropic exponential covariance, and no correlation exists between the layers. The variances and correlation lengths are all assumed to be 0.6 and 200 m, respectively. The top and bottom boundaries are no-flow, and the right and left sides are constant heads of 737 and 1000 m, respectively. The source line of 50 m long aligns vertically close to the left boundary. Six different locations of the source line, shown in the figure, are chosen for sensitivity studies. The CP is fixed near the right boundary. The irregularity of flow lines is caused by the rough layer boundaries and large difference of mean permeability between the layers. The mean flow lines also show that the groundwater mainly flows through the high-conductivity layers.

Fig. 11a and b shows the mean solute breakthrough curves and variances about the means with the source line at different locations. Generally speaking, the variance is proportional to the mean value. The solute travels fastest when the source line is between 850 and 900 m, and slowest with the source line between 100 and 150 m. This is consistent with the flow-line trajectory. When the solute goes to the fast channel, the solute has a fast mean movement and small dispersion, vice versa for the slow channel. Though not shown in the figure, one could imagine that with the increase of the size of the source line, the solute dispersion significantly increases owing to the strong heterogeneity in the vertical direction. The predicted standard deviation values are significantly larger than the mean values, indicating that the mean prediction may significantly deviate from the real solute transport. To decrease the variance, conditioning on field measurements may be required.

The results in Figs. 10 and 11 exhibit the flexibility of the moment method to solute transport in complex flow conditions. Further, the moment method greatly reduces the numerical calculation comparing with the Monte Carlo simulation method, since only ‘one realization’ calculation is required. Therefore, for the case under study the moment method is much more efficient than the Monte Carlo simulation method. It can be used as a screening tool to study the influences of the spatial variations of many parameters on solute

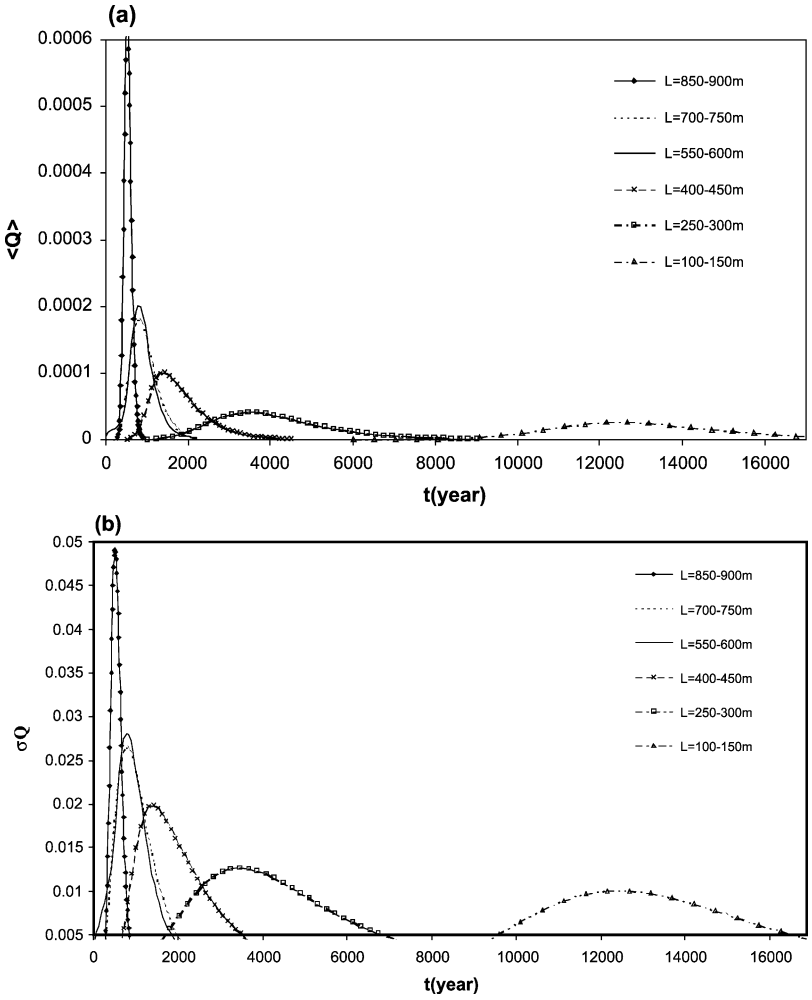

Fig. 11. Solute breakthrough curves with various source locations: (a) expected values and (b) standard deviations.

transport, and identify the most important factors for further investigation by other approaches.

7. Summary and discussion

In this paper, the nonstationary transport theory of Zhang et al. (2000) was made use of in studying solute flux through spatially nonstationary flows in porous media. The causes of flow nonstationarity include multi-scale and nonstationary medium features as well as complex hydraulic boundary conditions (Zhang, 2001). These nonstationary cases are not within the scope of the classical stochastic theory for stationary flow fields (Gelhar and Axness, 1983; Dagan, 1982, 1984; Dagan et al., 1992], but widely exist in natural fields. The stochastic frames for flow and transport are set up through analytical approaches, and numerical methods are utilized to obtain the solutions due to the complexity of the conductivity field, and initial and boundary conditions. This method, on one hand, greatly decreases the computational requirement in comparison with the Monte Carlo numerical simulation method; on the other hand, it can predict the flow and transport in much more complex subsurface environments than

the classical theory. The method used in this study provides a practical tool for applying stochastic approach to solute transport in complicated hydraulic conditions.

In this study, the effects of conductivity nonstationarity, hydraulic boundary and initial plume distribution on solute flux were investigated. The conductivity nonstationarity includes the spatial variations of the mean and correlation structure. Both of them have significant influence on the prediction of the mean and variance of the solute flux. For the cases studied, the predicted peak values of σ_Q and σ_q are larger than these of $\langle Q \rangle$ and $\langle q \rangle$, respectively, which implies that the prediction based on the mean value may significantly differ from the real transport process. Further, for all the case studies, if one compares the relative uncertainty, one may find $\sigma_Q/\langle Q \rangle \langle \sigma_q/\langle q \rangle$. As well known in the literature, $\langle Q \rangle$ is a more robust quantity than $\langle q \rangle$ but the former reveals less information than the latter.

Flow nonstationarity may significantly change the characteristics of the solute breakthrough curves. As a result, the mean and variance profiles may vary with time from a one-peak to bi-peak distribution.

In this study, the variation of conductivity correlation across the boundary between different media was considered. It was shown based on the examples chosen that the solute transport is very sensitive to the conductivity correlation across different media.

For the classical analytical stochastic methods (Gelhar and Axness, 1983; Dagan, 1982, 1984; Deng et al., 1993], the initial plume distribution is required to be as simple as a point or uniform distributed rectangle. The method used in this study can deal with any geometry of source shape and with any spatial density distribution. From Eqs. (2) and (4), one may notice that the particle distribution density functions, f_1 and f_2, are separated from the plume initial distribution, and the evaluation of density functions are the most time-consuming part of the calculation in this method. Therefore, the effort for computing solute flux moments will not significantly increase as the initial plume distribution is becoming more complex.

The moment method was applied to some hypothetical scenarios of solute transport in the groundwater below the Yucca Mountain project area. It was shown on the basis of the cases considered that the method is flexible in handling complex flow and solute transport conditions and has the computational efficiency in comparison with the Monte Carlos simulation method. Therefore, the method may provide a computational tool for many environmental projects under realistic conditions.

Acknowledgements

This work was supported in part by NSFC (project number 40272106) and by the Teaching and Research Award Program for Outstanding Young Teacher (TRAPOYT) of MOE, P.R.C.

References

Andricevic, R., Cvetkovic, V., 1998. Relative dispersion for solute flux in aquifer. J. Fluid Mech. 361, 145–174.

Bellin, A., Rubin, Y., Rinaldo, A., 1994. Eulerian–Lagrangian approach for modeling of flow and transport in heterogeneous geological formations. Water Resour. Res. 30, 2913–2925.

Cushman, J.H., 1997. The Physics of Fluids in Hierarchical Porous Media: Angstroms to Miles, Kluwer Academic.

Cvetkovic, V., Cheng, H., Wen, X.-H., 1996. Analysis of nonlinear effects on tracer migration in heterogeneous aquifers using Lagrangian travel time statistics. Water Resour. Res. 32, 1671–1681.

Dagan, G., 1982. Stochastic modeling of groundwater flow by unconditional and conditional probabilities, 2, The solute transport. Water Resour. Res. 18 (4), 835–848.

Dagan, G., 1984. Solute transport in heterogeneous porous formation. J. Fluid Mech. 145, 151–177.

Dagan, G., 1989. Flow and Transport in Porous Formayions, Springer-Verlag, New York.

Dagan, G., Cvetkovic, V., Shapiro, A.M., 1992. A solute flux approach to transport in heterogeneous formation, 1, The general framework. Water Resour. Res. 28, 1369–1376.

Deng, F.-W., Cushman, J.H., Delleur, J.W., 1993. A fast Fourier transform stochastic analysis of the contaminant transport problem. Water Resour. Res. 29 (9), 3241–3247.

Gelhar, L.W., 1993. Stochastic Subsurface Hydrology, Prentice-Hall, Englewood Cliffs, NJ.

Gelhar, L.W., Axness, C.L., 1983. Three-dimensional stochastic analysis of macrodispersion in aquifers. Water Resour. Res. 19, 161–180.

Graham, W., McLaughlin, D., 1989a. Stochastic analysis of nonstationary subsurface solute transport: 1. Unconditional moments. Water Resour. Res. 25 (2), 215–232.

Graham, W., McLaughlin, D., 1989b. Stochastic analysis of nonstationary subsurface solute transport: 2. Conditional moments. Water Resour. Res. 25 (11), 2331–2355.

Hess, K.M., 1989. Use of a borehole flowmeter to determine spatial heterogeneity of hydraulic conductivity and macrodispersivity in a sand and gravel aquifer, Cape Cod, Massachusetts. In: Molz, F.J., Melville, J.G., Guven, O. (Eds.), Proceeding of the Conference on New Field Techniques for Quantifying the Physical and Chemical Properties of Heterogeneous Aquifers, National Water Well Association, Dublin, Ohio, pp. 497–508.

Indelman, P., Rubin, Y., 1995. Flow in heterogeneous media displaying a linear trend in log conductivity. Water Resour. Res. 31, 1257–1265.

Indelman, P., Yubin, Y., 1996. Solute transport in nonstationary velocity fields. Water Resour. Res. 32, 1259–1267.

Li, S.-G., McLaughlin, D., 1995. Using the nonstationary spectral method to analyze flow through heterogeneous trending media. Water Resour. Res. 31, 541–551.

Rubin, Y., Seong, K., 1994. Investigation of flow and transport in certain cases of nonstationary conductivity fields. Water Resour. Res. 30, 2901–2911.

Shirley, C., Pohlmann, K., Andricevic, R., 1997. Three-dimensional mapping of equiproble hydrostratigraphic units at the French-man Flat corrective action unit, Nevada Test Site, Desert Research Institute, Report No. 45152,.

Sudicky, E.A., 1986. A natural gradient experiment on solute transport in a sand aquifer: Spatial variability of hydraulic conductivity and its role in the dispersion process. Water Resour. Res. 22 (13), 2069–2082.

Zhang, D., 1998. Numerical solutions to statistical moment equations of groundwater flow in nonstationary, bounded heterogeneous media. Water Resour. Res. 34, 529–538.

Zhang, D., 2001. Stochastic Methods for Flow in Porous Media: Coping with Uncertainties, Academic Press, San Diego, Calif.

Zhang, D., Winter, C.L., 1999. Moment equation approach to single phase fluid flow in heterogeneous reservoirs. SPEJ Soc. Pet. Eng. J. 4 (2), 118–127.

Zhang, D., Andricevic, R., Sun, A.Y., Hu, B.X., He, G., 2000. Solute flux approach to transport through spatially nonstationary flow in porous media. Water Resour. Res. 36, 2107–2120.

Zyvoloski, G.A., Robinson, B.A., Birdsell, K.H., Gable, C.W., Czarnecki, J., Bower, K.M., Faunt, C., 1997. Saturated Zone Radionuclide Transport Model, Yucca Mountain, Nevada, Los Alamos National Laboratory YMP Milestone SP25CM3A,.